Ballistic Transport in Carbon Nanotubes from First-Principles Molecular Dynamics Simulations

Young-Su Lee,[1] Marco Buongiorno Nardelli,[2] and Nicola Marzari[1]
[1]Department of Materials Science and Engineering, MIT, Cambridge MA 02139
and Institute for Soldier Nanotechnologies, MIT, Cambridge MA 02139
[2]Department of Physics, North Carolina State University, Raleigh NC 27695
and CCS-CSM, Oak Ridge National Laboratory, Oak Ridge, TN 37831

***Abstract*— We determined the Landauer ballistic conductance of pristine nanotubes at finite temperature via a novel scheme that combines ab-initio molecular dynamics, maximally-localized Wannier functions, and a tight-binding formulation of electronic transport in nanostructures. Large-scale ab-initio molecular dynamics simulations are used to obtain efficiently accurate trajectories in phase space. The extended Bloch orbitals for states along these trajectories are converted into maximally-localized orbitals, providing an *exact* mapping of the ground-state electronic structure onto a short-ranged Hamiltonian. Green's functions, self-energies, and ballistic conductance can then be obtained for any given configuration, and averaged over the appropriate statistical ensemble.**

***Index Terms*— Carbon nanotubes and nanostructures, Landauer conductance, first-principles, Wannier functions.**

I. Introduction

FIRST-PRINCIPLES simulation techniques are very natural tools to probe the properties of matter at the nanoscale, since they derive macroscopic properties from a detailed and fundamental quantum mechanical description of all the electrons interacting with the atomic nuclei. In doing so, they combine their fundamental quantum-mechanical predictive power with atomic resolution in length and time. We use here extensively these techniques in order to develop a microscopic understanding of the transport properties of nanosized object (carbon nanotubes), and to provide testing and guidance for their design and functionalization toward target applications. Three fundamental steps are needed to determine the transport characteristics of a nanostructure. Maximally-localized Wannier functions: The first-principles molecular dynamics algorithm evolves "on-the-fly" the electronic structure of the system, in both the occupied and the unoccupied subspace. Since we are studying extended or semi-infinite systems (the leads), and due to the use of periodic boundary conditions, the orbitals are in their Bloch extended form. The Bloch representation is not useful to calculate the conductance (see below), but using the Marzari-Vanderbilt maximally-localized Wannier functions approach [1] [2] we can determine the optimal unitary rotations at every point in the Brillouin zone that transform the extended orbitals into localized Wannier functions, preserving the same identical Hilbert space (i.e. we are performing a unitary transformation on the orbitals that localizes them as much as possible). Real-space Hamiltonian: In addition, the Hamiltonian matrix based on extended Bloch orbitals is converted to the real-space Hamiltonian with maximally-localized Wannier functions basis. Quantum conductance: The Landauer conductance is then calculated from the Green's functions of the conductor and its coupling to the leads (via the self- energies). Namely, the conductance G of the full system is given by $G = 2e^2/hTr(\Gamma_L G_C \Gamma_R G_C)$, where G_C is the Green's function of the conductor, and $\Gamma_{L,R}$ are the coupling functions that describe the interaction between the conductor and the leads. These can be calculated from the retarded and advanced self-energies, using the formalism of principal layers and the surface Green's function matching theory briefly outlined below, and exploiting the decomposition into localized orbitals obtained from the maximally-localized representation (see Refs. [3] and [4]). The Green's function is also obtained straightforwardly in a localized orbital scheme from the Hamiltonian and overlap matrices.

These steps are carried out in detail using as paradigmatic cases (8,0) semiconducting and (5,5) metallic single-wall carbon nanotubes (or SWCNT). Several experimental findings reported ballistic transport for carbon nanotubes even at room temperature and at micrometer length scales [5][6]. Also, their different electrical properties and functionalization avenues with organic and biological molecules promise a wide variety of applications in nanoelectronics [7][8][9].

In our electronic structure calculations we use Car-Parrinello molecular dynamics based on ultrasoft pseudopotentials[10], density-functional theory in the PBE-GGA approximation, and we use a planewave basis set with a wavefunction cutoff of 30 Ry and a charge density cutoff of 240 Ry. Our supercells contain 96 atoms for the (8,0) SWCNT, corresponding to three layers of the conventional unit cell for the (8,0) SWCNT, and 100 atoms for the (5,5) SWCNT, corresponding to five layers of the conventional unit cell. Such supercell sizes are large enough to allow for Γ-sampling only in the Brillouin zone, and to have negligible overlap with the maximally-localized Wannier functions belonging to the second next supercell (see Section III for details).

Nicola Marzari has been partially supported by the Singapore-MIT Alliance
Nicola Marzari is with the Department of Materials Science of the Massachusetts Institute of Technology, Cambridge, MA 02139 USA (telephone: 617-4522758, e-mail: marzari@mit.edu)

II. Maximally-localized Wannier functions

A. General Formalism

Electronic structure calculations are often carried out using periodic boundary conditions, this is the most natural choice to study perfect crystals and to minimize finite size-effects in the study of several non-periodic systems (e.g. surfaces, impurities, or the lead-conductor-lead geometries considered here). The one-particle effective Hamiltonian $\hat{H}$ then commutes with the lattice-translation operator $\hat{T}_{\mathbf{R}}$, allowing one to choose as common eigenstates the Bloch orbitals $|\,\psi_{n\mathbf{k}}\,\rangle$:

$$[\,\hat{H},\,\hat{T}_{\mathbf{R}}\,]\;=\;0\;\;\Rightarrow\;\;\psi_{n\mathbf{k}}(\mathbf{r})\;=\;e^{i\phi_n(\mathbf{k})}\,u_{n\mathbf{k}}(\mathbf{r})\,e^{i\mathbf{k}\cdot\mathbf{r}}\;\;,\quad(1)$$

where $u_{n\mathbf{k}}(\mathbf{r})$ has the periodicity of the Hamiltonian. There is an arbitrary phase $\phi_n(\mathbf{k})$, periodic in reciprocal space, that is not assigned by the Schrödinger equation and that we have written out explicitly. We obtain a (non-unique) Wannier representation using any unitary transformation of the form $\langle\, n\mathbf{k}\,|\,\mathbf{R}n\,\rangle = e^{i\varphi_n(\mathbf{k})-i\mathbf{k}\cdot\mathbf{R}}$:

$$|\,\mathbf{R}n\,\rangle\;=\;\frac{V}{(2\pi)^3}\;\int_{BZ}|\,\psi_{n\mathbf{k}}\,\rangle\,e^{i\varphi_n(\mathbf{k})-i\mathbf{k}\cdot\mathbf{R}}\,d\mathbf{k}\;\;.\quad(2)$$

Here V is the real-space primitive cell volume. It is easily shown that the $|\,\mathbf{R}n\,\rangle$ form an orthonormal set, and that two Wannier functions $|\,\mathbf{R}n\,\rangle$ and $|\,\mathbf{R}'n\,\rangle$ transform into each other with a translation of a lattice vector $\mathbf{R}-\mathbf{R}'$[11]. The arbitrariness that is present in $\varphi_n(\mathbf{k})$ [or $\phi_n(\mathbf{k})$] propagates to the resulting Wannier functions, making the Wannier representation non-unique. Since the electronic energy functional in an insulator is also invariant with respect to a unitary transformation of its n occupied Bloch orbitals, there is additional freedom associated with the choice of a full unitary matrix (and not just a diagonal one) transforming the orbitals between themselves at every wavevector $\mathbf{k}$. Thus, the most general operation that transforms the Bloch orbitals into Wannier functions is given by

$$|\,\mathbf{R}n\,\rangle\;=\;\frac{V}{(2\pi)^3}\;\int_{BZ}\sum_m U^{(\mathbf{k})}_{mn}\,|\,\psi_{m\mathbf{k}}\,\rangle\,e^{-i\mathbf{k}\cdot\mathbf{R}}\,d\mathbf{k}\;\;.\quad(3)$$

The Wannier functions $w_n(\mathbf{r}-\mathbf{R})\;=\;|\,\mathbf{R}n\,\rangle$, for non-pathological choices of phases, are "localized": for a $\mathbf{R}_i$ far away from $\mathbf{R}$, $w_n(\mathbf{R}_i-\mathbf{R})$ is a combination of terms like $\int_{BZ}\,u_{m\mathbf{k}}(0)e^{i\mathbf{k}\cdot(\mathbf{R}_i-\mathbf{R})}\,d\mathbf{k}$, which are small due to the rapidly varying character of the exponential factor [11].

B. Γ-point Formalism

For isolated systems and insulating crystals, it is appropriate to use only the wavefunctions at the Γ-point of BZ to construct maximally-localized Wannier functions - provided the unit cell is large enough. In this case, Eq.(3) is reduced to a simple unitary transformation.

$$|w_n\rangle=\sum_m U_{mn}\,|\,\psi_m\,\rangle\quad(4)$$

We define the overlap matrices

$$M^l_{ij}=\langle w_i|e^{-i\mathbf{G}_l\cdot\mathbf{r}}|w_j\rangle,\quad(5)$$

(where $\mathbf{G}_l$ are the reciprocal lattice vectors of the unit cell, and w_j the Γ point wavefunctions), a functional S can be constructed:

$$S=\sum_{i=1}^{N}\sum_{l=1}^{N_G}\,W_l\,|M^l_{ii}|^2\quad(6)$$

(N is the number of bands, N_G is the number of the $\mathbf{G}_l$ vectors required to preserve the natural symmetry, and W_l is the weight corresponding to the specific vector $\mathbf{G}_l$). This quantity is closely related to the spread of the Wannier functions, which measures their delocalization:

$$\begin{aligned}\Omega\;&=\;(\frac{L}{2\pi})^2\sum_{i=1}^{N}\sum_{l=1}^{N_G}\,W_l\,[\,\langle\omega_i|(\mathbf{G}_l\cdot\mathbf{r})^2|\omega_i\rangle-\langle\omega_i|\mathbf{G}_l\cdot\mathbf{r}|\omega_i\rangle^2\,]\\&=\;(\frac{L}{2\pi})^2\,\sum_{i=1}^{N}\sum_{l=1}^{N_G}\,W_l\,(1-|\langle\omega_i|e^{-i\mathbf{G}_l\cdot\mathbf{r}}|\omega_i\rangle|^2\,)+O(L^{-2})\\&=\;(\frac{L}{2\pi})^2\,(\sum_{i=1}^{N}\sum_{l=1}^{N_G}\,W_l-S)+O(L^{-2})\;,\end{aligned}\quad(7)$$

where L is the supercell dimension. Instead of minimizing the spread we can maximize the functional S; the Wannier function center of the i-th occupied band $\mathbf{r}_i$ is then computed using:

$$\mathbf{r}_i=-(\frac{L}{2\pi})^2\,\sum_l\,W_l\,\mathbf{G}_l\,Im\ln M^l_{ii}.\quad(8)$$

Fig.1 shows Wannier functions of semiconducting and metallic SWCNTs. For (8,0) SWCNT, we are able to convert delocalized valence band Bloch orbitals to a set of σ and bonding π type Wannier functions.

The case of conduction bands needs to be dealt with more care, since these are usually an entangled subspace that can't be separated from the higher bands not considered in the calculation. However, we can obtain Wannier-like well-localized orbitals applying the disentanglement procedure developed by Souza et al.[2]. The spread of Wannier functions can usually be decomposed into two components[1].

$$\Omega=\Omega_{\mathbf{I}}+\widetilde{\Omega}\quad(9)$$

$\Omega_{\mathbf{I}}$ is *gauge-invariant* in a semiconductor or an insulator, and thus the unitary transformations in Eq.(4) only affect (and minimizes) $\widetilde{\Omega}$. A subspace with optimal "smoothness" can be disentangled from the conduction band structure by selecting the linear combination of orbitals that has maximal inter-orbital overlap [2]; this is equivalent to maximizing $\Omega_{\mathbf{I}}$ in the case of a metal. Once the optimally-connected subspace has been extracted, the localization procedure follows the same steps as for an isolated band calculation.

In case of the (8,0) SWCNT, 48 identical anti-bonding π^* Wannier-like functions can be easily disentangled from the conduction band using the procedure we alluded to above. For truly metallic system, even the occupied space is entangled with the unoccupied space, requiring a global disentangling procedure. For our (5,5) SWCNT with 100 carbon atoms, we start with 300 Bloch orbitals and then construct a connected subspace of 250 orbitals; the localization procedure that follows results in 150 sp^2 orbitals and 100 p_z orbitals, as shown in Fig.1

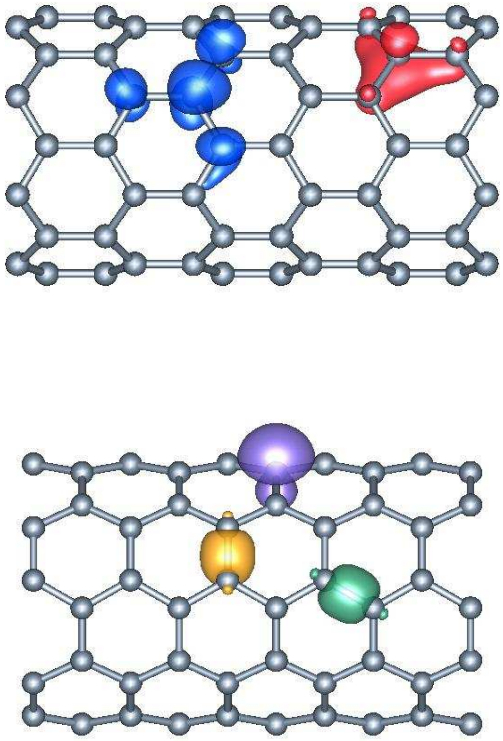

Fig. 1. Upper panel : charge density of bonding π (right) and anti-bonding π^* (left) Wannier functions in the (8,0) SWCNT. Lower panel : charge density of sp^2 and p_z Wannier functions in the (5,5) SWCNT.

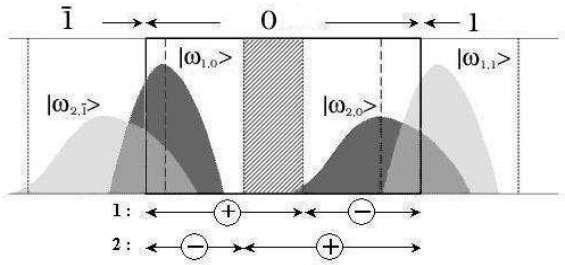

Fig. 2. Schematic description of our real-space integration technique: The "real" Wannier functions **1** and **2** are marked in dark gray, and their periodic translation in light gray. $\oplus$ is an effective overlap region defined by $[z_i - L/2, z_i + L/2]$ inside 0th cell. Only the middle part, where the $\oplus$ region of **1** **2** overlap contributes to $H_{00,12}$.

III. Real-space Hamiltonian

A. Unitary transformations of the Hamiltonian

Any solid (or surface) can be viewed as an infinite (or semi-infinite in the case of surfaces) stack of "principal layers" interacting only with their neighboring layers. [12]. Within this approach, the infinite-dimensional real-space Hamiltonian can be divided into the finite-sized Hamiltonian matrices. In case of a bulk system (i.e. infinite and periodic) the only independent components are H_{00} and H_{01}, where the former represents the interaction between orbitals located in the same principal layer and the latter the interaction between orbitals in one principal layer and the next. In our formulation, the real-space basis orbitals are provided by the maximally-localized Wannier functions and the supercell corresponds to one single principal layer.

We want to elaborate here on a technical issue arising from the use of Γ-point sampling. If a unit cell has a length L, and its Brillouin zone is sampled with N $\mathbf{k}$-points along that same direction, the real-space Bloch orbitals will display $N*L$ periodicity. For N reasonably large, the periodic images of the localized Wannier orbitals will be located far apart, and thus the interaction with a ghost periodic image will be negligible[13]. However, the restriction to Γ-point sampling means that even localized orbitals are repeated periodically from supercell to supercell - thus, we need to avoid spurious overlap terms in our Hamiltonian. The nth cell for each Wannier function is chosen as $[z_i - L/2 + nL, z_i + L/2 + nL]$, where z_i is the z-coordinate of Wannier function center from Eq.(8) and the system is infinite along z-axis. We reorganize the Hamiltonian matrix by neglecting any interaction between Wannier functions $|\omega_{i,n}\rangle$ and $|\omega_{j,m}\rangle$ apart by more than two times of the unit cell length L.

$$\begin{aligned}\langle w_i|\hat{H}|w_j\rangle &= \sum_{n=-\infty}^{\infty}\langle\omega_{i,0}|\hat{H}|\omega_{j,n}\rangle \qquad (10)\\ &= \langle\omega_{i,0}|\hat{H}|\omega_{j,\bar{1}}\rangle + \langle\omega_{i,0}|\hat{H}|\omega_{j,0}\rangle + \langle\omega_{i,0}|\hat{H}|\omega_{j,1}\rangle\\ &= H_{\bar{1}0,ij} + H_{00,ij} + H_{01,ij}\\ &= H^{\dagger}_{01,ij} + H_{00,ij} + H_{01,ij}\end{aligned}$$

In practice, a matrix element $H_{00,ij}$ is determined with an integration on a real space grid. Let's take as an example the calculation of $H_{00,12}$ and $H_{01,12}$ for the Wannier Functions **1** and **2** pictured in Fig. 2. $H_{00,12}$ will have zero value, since there is negligible overlap between $|\omega_{1,0}\rangle$ and $|\omega_{2,0}\rangle$. However, $\langle w_1|\hat{H}|w_2\rangle$ is appreciable because of the interaction between $\omega_{2,0}\rangle$ and $\omega_{1,1}\rangle$. By assumption, $H_{\bar{1}0,12}$ is set to zero. The decomposition of $\langle w_1|\hat{H}|w_2\rangle$ into two components, $H_{00,12}$ and $H_{01,12}$, is done as follows: The integrated value in real-space on those grids belonging to the "true" overlap region of both Wannier functions (highlighted in gray in Fig. 2, adds on to $H_{00,12}$, while the rest adds on to $H_{01,12}$. As an example, we plot H_{00} and H_{01} in Fig.3, on a logarithmic scale. It can be clearly seen that the interaction term decreases exponentially as the distance between Wannier functions increases.

B. Band Structure

Orthonormal Bloch orbitals for any arbitrary $\mathbf{k}$ point can be obtained by Fourier interpolations of the Wannier functions. This is done in complete analogy to a tight-binding formulation - but in our case the basis set provided by the Wannier functions results in an *exact* mapping of the ground-state electronic structure:

$$\psi_i^{\mathbf{k}}(r) = \frac{1}{\sqrt{N_R}}\sum_{\mathbf{R}} e^{i\mathbf{k}\cdot\mathbf{R}}\omega_i(r-\mathbf{R})\ ; \qquad (11)$$

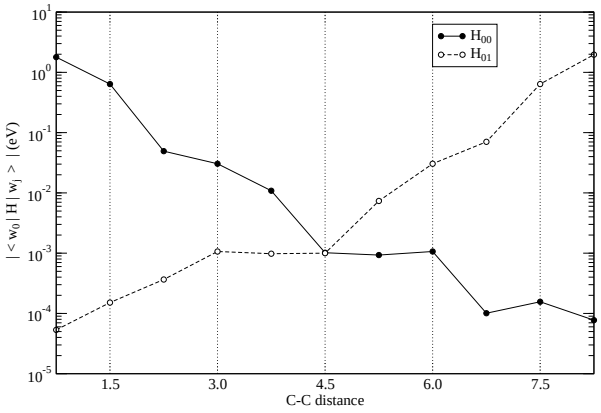

Fig. 3. H_{00} and H_{01} as a function of distance between σ type Wannier functions of (8,0) SWCNT

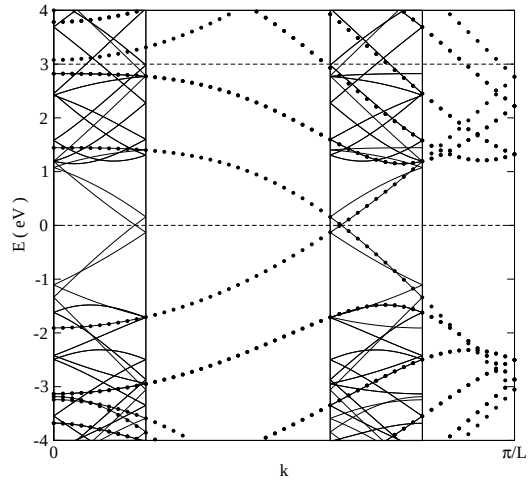

Fig. 4. Comparison of band structures calculates from maximally-localized Wannier orbitals in a supercell calculation, and a full diagonalization of the Hamiltonian, for a (5,5) SWCNT

conversely, the Hamiltonian matrix is:

$$\langle\psi_i^{\mathbf{k}}|\hat{H}|\psi_j^{\mathbf{k}}\rangle = H_{00,ij} + e^{i\mathbf{k}\cdot\mathbf{R}}H_{01,ij} + e^{-i\mathbf{k}\cdot\mathbf{R}}H_{01,ij}^{\dagger}\ , \quad (12)$$

where we have exploited the short-rangedness of our orbitals. Fig. 4 shows the band structure of a (5,5) SWCNT, with the solid lines calculated diagonalizing the above Hamiltonian matrix at any given $\mathbf{k}$ point, and the circles from a full band-structure calculation using a publicly-available electronic-structure code (PWSCF [14]). The Brillouin zone of the supercell calculation corresponds to one fifth of that in the conventional unit cell. The excellent agreement between two methods proves that our approach exactly maps the reciprocal-space Hamiltonian matrix into an real-space one without any accuracy loss.

IV. Quantum Conductance

Our final goal is to calculate the quantum conductance following the procedure outlined in Introduction. Here, we apply the quantum conductance formalism of Nardelli [3], which is applicable to any general Hamiltonian described within a localized orbital basis. We consider a system composed of a conductor C connected to two semi-infinite leads, R and L. The conductance through a region of interacting electrons is related to the scattering properties of the region itself via the Landauer formula [15]:

$$\mathcal{G}(E) = \frac{2e^2}{h}\mathcal{T}(E), \quad (13)$$

where $\mathcal{T}$ is the transmission function and $\mathcal{G}$ is the conductance. $\mathcal{T}$ is the probability that an electron injected at one end of the conductor will transmit to the other end. This transmission function can be expressed in terms of the Green's functions of the conductors and the coupling of the conductor to the leads [16], [17]:

$$\mathcal{T} = \mathrm{Tr}(\Gamma_L G_C^r \Gamma_R G_C^a), \quad (14)$$

where $G_C^{\{r,a\}}$ are the retarded and advanced Green's functions of the conductor, and $\Gamma_{\{L,R\}}$ are functions that describe the coupling of the conductor to the leads. To compute the Green's function of the conductor we start from the equation for the Green's function of the whole system:

$$(\epsilon - H)G = I \quad (15)$$

where $\epsilon = E + \mathrm{i}\eta$ with η arbitrarily small and I is the identity matrix.

In the hypothesis of leads and conductors being of the same material (bulk conductivity), expression for the Green's function of infinite system is:

$$\begin{pmatrix} G_L & G_{LC} & G_{LCR} \\ G_{CL} & G_C & G_{CR} \\ G_{LRC} & G_{RC} & G_R \end{pmatrix} = \quad (16)$$

$$\begin{pmatrix} (\epsilon - H_L) & H_{01} & 0 \\ H_{01}^{\dagger} & (\epsilon - H_{00}) & H_{01} \\ 0 & H_{01}^{\dagger} & (\epsilon - H_R) \end{pmatrix}^{-1},$$

We can write the bulk Green's function as:

$$G(E) = (\epsilon - H_{00} - H_{01}T - H_{01}^{\dagger}\overline{T})^{-1}. \quad (17)$$

where T and $\overline{T}$ are the transfer matrices, which are defined such that $G_{10} = TG_{00}$ and $G_{00} = \overline{T}G_{10}$. The transfer matrices are calculated following the iterative procedure by Lopez-Sancho et al.[18]. In particular, the last two terms in Eq.(17), $H_{01}^{\dagger}\overline{T}$ and $H_{01}T$ imply the coupling between the conductor with the semi-infinite left and right side of bulk material. The knowledge of the bulk Green's function G also gives direct informations on the electronic spectrum via the spectral density of bulk electronic states: $N(E) = -(1/\pi)\mathrm{Im}(\mathrm{Tr}G(E))$.

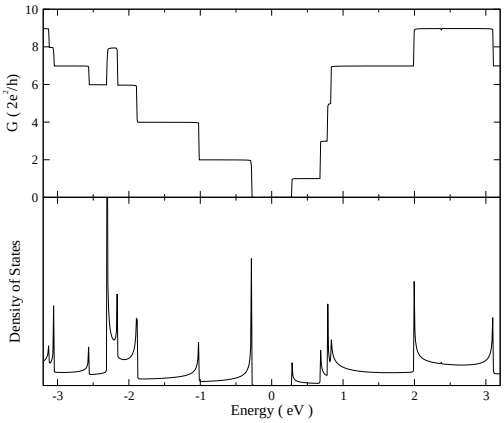

Fig. 5. Quantum conductance and density of states for a (8,0) SWCNT

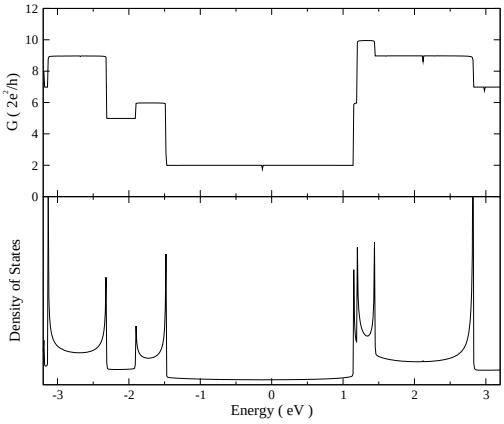

Fig. 6. Quantum conductance and density of states for a (5,5) SWCNT

A. Results for ideal SWCNT

We show in Figs. 5 and 6 our results for the density of states and conductance for the two nanotubes examined.

In particular, the metallic nanotube, notwithstanding its 2 eV pseudo-gap at Γ, shows a band structure (Fig. 4) and a quantum conductance (Fig. 6) typical of a metallic system, and which manifest itself as two eigen-channels around the Fermi energy and a finite density of states. These characteristics would have not been apparent without the eigen-states interpolation between HOMO and LUMO at Γ via the localized Wannier functions.

B. Finite temperature effect

To investigate the effects of a finite temperature, we extracted twelve snapshots of our (5,5) metallic nanotube during a Car-Parrinello molecular dynamics simulation at 300K. Since the electronic structure of metallic nanotubes is susceptible to structural perturbations[19][20], finite temperature

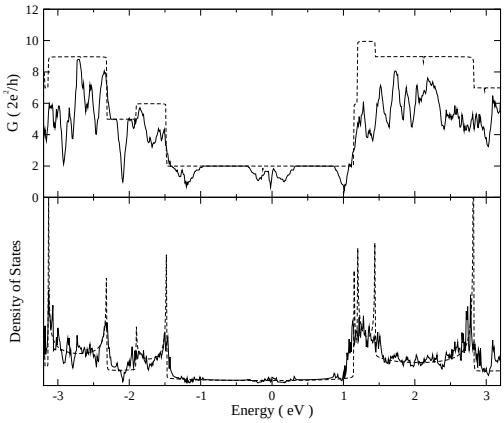

Fig. 7. Average quantum conductance of a (5,5) SWCNT at 300 K

vibrations could significantly affect the quantum conductance. We observe a consistent opening of mini-gaps around the Fermi energy.

V. Conclusion

In conclusion, we have developed a very efficient scheme to calculate the quantum transport of nanostructures directly from first-principles molecular dynamics simulations. As a benchmark system, ideal semiconducting and metallic SWCNT have been studied, showing perfect agreement for the band structure and the density-of-states with those calculated with traditional approaches on small supercells. Our method is generally applicable to large-scale simulations, and thus will prove invaluable in assessing the quantum conductance of realistic systems.

A. Acknowledgments

This research was supported by the U.S. Army through the Institute of Solider Nanotechnologies, under Contract DAAD-19-02-D0002 with the U.S. Army Research Office (Y.S.L and N.M.), the Singapore-MIT alliance, and the Mathematical, Information and Computational Sciences Division, Office of Advanced Scientific Computing Research of the U.S. Department of Energy under contract No. DE-AC05-00OR22725 with UT-Battelle (M.B.N.).

References

[1] N. Marzari and D. Vanderbilt, Phys. Rev. B **56**, 12847-12865 (1997).
[2] I. Souza, N. Marzari, and D. Vanderbilt, Phys. Rev. B **65**, 035109 (2002).
[3] M. Buongiorno Nardelli, Phys. Rev. B **60**, 7828-7833 (1999).
[4] M. Buongiorno Nardelli, J.-L. Fattebert, and J. Bernholc, Phys. Rev. B **64**, 245423 (2001).
[5] S. Frank, P. Poncharal, Z. L. Wang and W. A. de Heer, Science **280**, 1744-1746 (1998).
[6] A. Javey, J. Guo, M. Lundstorm and H. Dai, Nature **424**, 654-657 (2003).
[7] F. Leonard and J. Tersoff, Phys. Rev. Lett. **88**, 258302 (2002).
[8] A. Hirsch, Angew. Chem. Int. Ed. **41**, 1853-1859 (2002).
[9] K. A. Williams, P. T. M. Veenhuizen, B. G. de la Torre, R. Eritja and C.Dekker, Nature **420**, 761 (2002).

[10] K. Laasonen, A. Pasquarello, R. Car, C. Lee, and David Vanderiblt, Phys. Rev. B **47** 10142 (1993).
[11] E.I. Blount, Solid State Physics **13**, 305 (1962).
[12] D. H. Lee and J. D. Joannopoulos, Phys. Rev. B **23**. 4988 (1981); **23**, 4997 (1981).
[13] A. Calzolari, N. Marzari, I. Souza and M. B. Nardelli, Phys. Rev. B (in press).
[14] S. Baroni, A. Dal Corso, S. de Gironcoli, and P. Giannozzi, http://www.pwscf.org.
[15] R. Landauer, Philos. Mag. **21**, 863 (1970).
[16] S. Datta, *Electronic Transport in Mesoscopic Systems*, Cambridge University Press, Cambridge (1995).
[17] D. S. Fisher and P. A. Lee, Phys. Rev. B **23**, 6851 (1981).
[18] M. P. Lopez-Sancho, J. M. Lopez-Sancho, and J. Rubio, J. Phys. F **14**, 1205 (1984); **15**, 851 (1985).
[19] C. L. Kane and E. J. Mele, Phys. Rev. Lett. **78**, 1932-1935 (1997).
[20] J.-Q. Lu, J. Wu, W. Duan, F. Liu B.-F. Zhu and B.-L. Gu, Phys. Rev. Lett. **90**, 156601 (2003).